The green light emission of CsPbBr$_3$ quantum-dots microcrystals with different concentrations of F$^-$ doping

YONGXIA LI, HAOWEN BAI, JIANG WU, GUANYING CAO[*], YANJIE ZHANG[*]
Research Institute of Photonics, Dalian Polytechnic University, Dalian 116034, China

CsPbBr$_3$ quantum-dots were successfully prepared in fluorine doped borosilicate microcrystals with different concentrations. The crystal structure of the perovskite quantum-dots was determined by XRD. The morphology of perovskite quantum-dots was characterized by TEM. The fluorescence characteristics were analyzed by fluorescence spectrum and CIE chromaticity coordinate. The XRD patterns show that the perovskite quantum-dots microcrystals were successfully doped in the borosilicate microcrystals. The TEM results show that CsPbBr$_3$ quantum-dots are uniformly distributed in borosilicate microcrystals. Under the excitation of 360 nm ultraviolet light, the CsPbBr$_3$ quantum-dots exhibit strong green emission at 519 nm. The lifetime decay of quantum-dot crystallites increased from 4.04 ns to 14.42 ns, and the PLQY reached 44.81%. Therefore, the obtained quantum-dots can be used in the powder solid-state light-emitting devices with high light efficiency and long-life span.

1. Introduction

Lead halide perovskite has become an advanced material in photovoltaic field due to its significant luminous efficiency [1]. In previous studies, organic-inorganic hybrid perovskite materials were mostly selected to improve the conversion efficiency of solar cells, such as lead methy lammonium iodide (MAPbI$_3$) and lead formamidine iodide (FAPbI$_3$) [2-3]. However, due to the extremely unstable cations, the hybrid perovskite has obvious disadvantages in thermal stability, which hinders its development [4]. In the further exploration, the inorganic perovskite was successfully prepared by replacing the organic component with inorganic Cs cations [5]. Nowadays, all inorganic CsPbX$_3$ (X = Cl, Br, I) perovskite quantum-dots(QDs) have become hot research topics among luminescent materials, due to its excellent optical properties, such as low exciton binding energy, tunable light emission, narrow emission linewidth, high photoluminescence (PL) efficiency, light absorption and high photoluminescence quantum yield (PLQY) [6-14]. In addition, CsPbBr$_3$ perovskite QDs are widely used in solar cells [15-18], light-emitting diodes [19-22], lasers [23-26], photodetectors [27], polarizers [28] and displays [29]. Comparing with the organic-inorganic hybrid perovskite, all types of inorganic perovskite exhibit better stability. However, in more complicated environments like air or high temperature, the stability of CsPbX$_3$ (X = Cl, Br, I) perovskite remains unsatisfied. In 2016, Bing Ai prepared CsPbBr$_3$ QDs in phosphate glass by traditional melting quenching and heat treatment methods, showing excellent luminescent performance [30]. In addition, CdS, CdSe and PbSe QDs were successfully prepared in glass, which proved that glass can promote the formation of internal QDs, greatly promoting the thermal and chemical stability of QDs [31-33].

In this study, for the low luminous efficiency and poor PLQY of perovskite QDs, by doping with fluoride, a uniform distribution of perovskite QDs crystallites in a glass matrix was successfully prepared. The amorphous structure of the glass inhibits the growth inside the QDs. Fluorinated glass changes the internal network structure of glass. The introduced F$^-$ enters the network structure by breaking the Si-O bond, and produces the bridging oxygen ion structure, which provides enough space for ion diffusion, thus promoting the precipitation of CsPbBr$_3$ QDs in the glass and improving the PLQY [34].

Compared with the perovskite QDs microcrystals that were not doped with fluoride before, the introduction of fluorine can effectively change the internal defects of borosilicate and promote the rapid growth of QDs [35]. Under the fluorescence spectrum and CIE chromaticity coordinate analysis, the sample showed excellent luminescence performance and better stability. This is an insightful discovery in the field of solid perovskite luminescent materials.

2. Experimental

2.1. Sample preparation

The reagents needed in the experiments are lead bromide (PbBr$_2$, 99%), cesium carbonate (Cs$_2$CO$_3$, 99%),

strontium carbonate ($SrCO_3$, 99%), strontium fluoride (SrF_2, 99%), sodium bromide (NaBr, 99%), boric acid (H_3BO_3, 99%), silica (SiO_2, 99%) and zinc oxide (ZnO, 99%). The raw glass and perovskite materials are fully grounded in the glove box, so as to isolate from the air during the whole process. The prepared sample was heated to 1180 °C under alumina at a heating rate of 10 °C / min

and for 10 min, then cooled to room temperature (about 20 °C) by different cooling methods at a precooling rate of 10 °C / min. Finally, the sample was calcined for a second time and kept warm for 5 h until cooled to room temperature. Fig. 1 shows the schematic illustration of the $CsPbBr_3$ QDs microcrystalline preparation process.
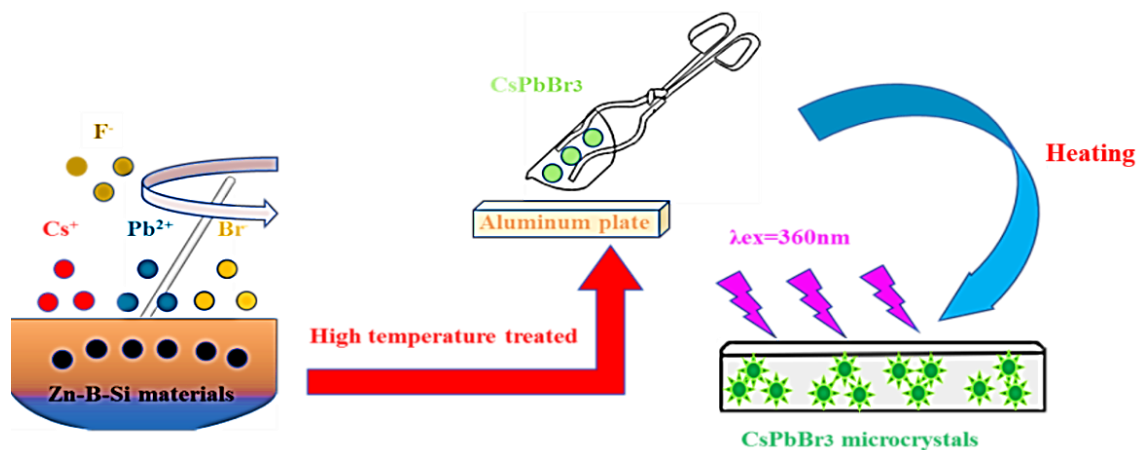
Fig. 1. CsPbBr₃ QDs microcrystalline preparation process diagram (color online)

2.2. Materials characterization

X-ray diffraction (XRD) was measured by Bruker-D8 advance measurement, equipped with a Cu Kα radiation flux, with voltage of 40 kV, current of 30 Ma, velocity of 0.02 °S^{-1} and boundary of 10°–70° (2θ). The microstructure of QDs was characterized by JEM-2100 field emission Transmission electron microscopy (TEM). The photoluminescence excitation spectrum and emission spectrum (slit: 1.0) of $CsPbBr_3$ QDs microcrystals were measured by 150 W xenon lamp fluorescence spectrometer F-7000 (220-240 V). The thermal stability of the material was measured by heating in KSL-1200X muffle furnace for 5 h. The yield and lifetime were obtained by a fluorescence spectrometer (FL-920). CIE chromaticity coordinates was used to represent the position of material chromaticity coordinates.

3. Results and discussion

3.1. XRD pattern of CsPbBr₃

The XRD diffraction patterns of $CsPbBr_3$ QDs microcrystals doped with different concentrations of F⁻ are shown in Fig. 2. The change trend of crystal structure of QDs doped with different concentrations of fluorine under heat treatment at 460 °C are shown in Fig. 2(a). Without F⁻ doping, the sample does not show obvious diffraction peaks. With the increase of F⁻ concentration, when the concentration is $SrCO_3$: SrF_2 = 3:7, the sample highlights weak diffraction peaks in the (200) and (211) planes. When all are replaced by pure SrF_2 doping, the sample shows obvious diffraction peaks. This reveals that

perovskite QDs are inhibited in the growth of borosilicate microcrystals. Due to the structural defects of borosilicate microcrystals, it is difficult for QDs to break through the internal network structure. Therefore, the diffraction peak of $CsPbBr_3$ QDs microcrystals is covered by the signal of disordered borosilicate microcrystals, so it is difficult to show obvious diffraction peaks. Fig. 2(b) is an XRD diagram of pure SrF_2 doped microcrystalline samples. It is found that the positions of the strongest diffraction peaks at 21.31°, 30.41° and 37.51° correspond to the planes of (110), (200) and (211) of $CsPbBr_3$ cubic phase standard card (PDF#54-0572). It is confirmed that the microcrystalline of $CsPbBr_3$ QDs formed in F-doped borosilicate microcrystals. Therefore, F⁻ doping can change the internal network structure of borosilicate microcrystals, providing enough space for ion diffusion and effectively promoting the formation of QDs. When calcined at 440 °C ~ 460 °C for 5 h, no diffraction peak was found. However, when the temperature gradually increased to 480 °C ~ 500 °C, there were obvious diffraction peaks. This is because the perovskite QDs fail to grow inside borosilicate microcrystals when the temperature is too low, most of them grow on the surface of microcrystals. With the increase of temperature, the radius of QDs cell increases and the growth gradually takes shape, which makes the yield of QDs microcrystalline in borosilicate increase. As shown in Fig. 2(b), at 500 °C, the microcrystalline diffraction peak of QDs is intense and narrow, which means that the PLQY is the highest. When the temperature is further increased, the diffraction peak is no longer obvious, because the high temperature leads to the extinction between the QDs, thus reducing the yield.
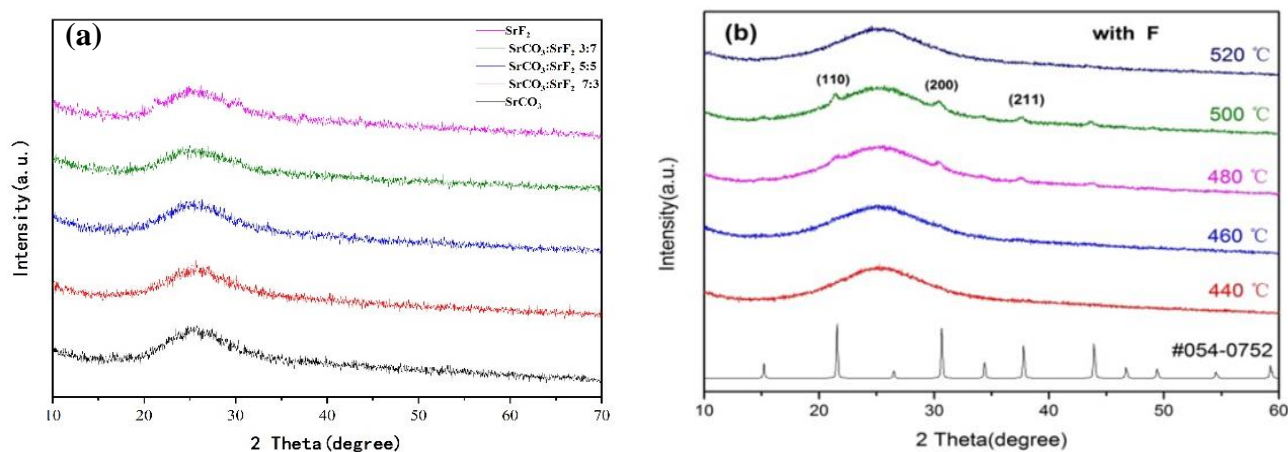
Fig. 2. XRD images of CsPbBr$_3$ QDs microcrystals under different concentrations (a) and temperatures (b) for 5 h heat treatment (color online)
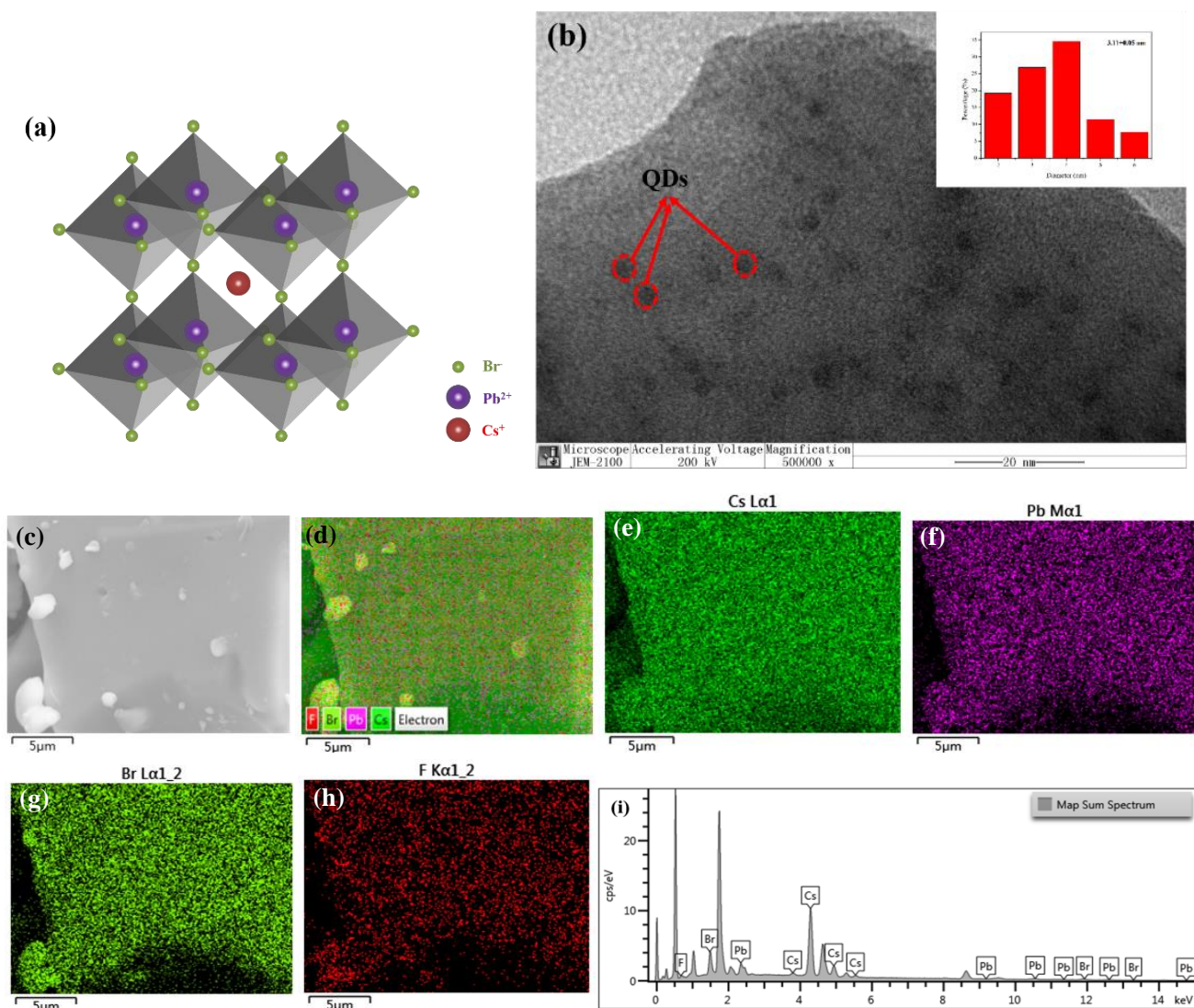
Fig. 3. (a) Schematic of the cubic perovskite lattice of CsPbBr$_3$; (b) TEM image of CsPbBr$_3$ QDs with heat treatment at 460 °C for 5 h. Inset: CsPbBr$_3$ QDs particle size distribution; (c) SEM image of CsPbBr$_3$ QDs; (d-h) The element distribution mapping of CsPbBr$_3$ QDs; (i) EDS spectrum of the CsPbBr$_3$ QDs (color online)

3.2. TEM and EDS pattern of CsPbBr₃

Fig. 3(a) shows the schematic of the cubic perovskite lattice of CsPbBr$_3$. Fig. 3(b) shows the TEM images of the green-emitting CsPbBr$_3$ QDs that were heat-treated at 460 °C for 5 h. QDs microcrystalline are widely distributed in the mixed fluoride glass substrate, and the average size of CsPbBr$_3$ QDs after statistics is 3.11 nm. Fig. 3(c) shows the SEM images of the green-emitting CsPbBr$_3$ QDs that were heat-treated at 460 °C for 5 h. TEM and SEM have demonstrated that QDs are successfully formed in the glass matrix. At the same time, as shown in Fig. 3(d-h), the uniform distribution of Cs/Pb/Br/F in the same particle region is confirmed by the energy dispersion spectrum element mapping. Fig. 3(i) is the QDs energy dispersion spectrogram. It can be clearly seen from the figure that doping F success fully promotes the growth of CsPbBr$_3$ QDs in the glass matrix.

3.3. Temperature-dependent luminescence properties

To explore F$^-$ doped with different concentrations of spectral adjustable, Fig. 4 shows the different concentration of F$^-$ in the spectrum of two kinds of heat treatment temperature movement regularity. Fig. 4(a) is an emission spectrum of different concentrations of F-doping

under heat treatment at 500 °C. It is obvious from the figure that under the irradiation of 365 nm ultraviolet light, the green light emission of the sample is the strongest when the concentration ratio is SrCO$_3$: SrF$_2$ = 3:7. Moreover, with the increase of fluorine ion concentration, the emission peak position of QDs microcrystalline shifts significantly. When the concentration is from pure SrCO$_3$ to SrCO$_3$: SrF$_2$ = 7:3, the emission peak blue shifts. When the F-concentration gradually increases to pure SrF$_2$ doping, the emission peak position has a clear red shifts, and the wave peak position moves to 524 nm, as shown in Fig. 4(b). In addition, in Fig. 4(a), when the concentration of F$^-$ gradually increases, the emission peak protruding around 460 nm gradually dissipates and tends to be stable. This may be due to the uneven particle size of CsPbBr$_3$ QDs [36]. Surprisingly, when the temperature is controlled at 460 °C, as shown in Fig. 4(c), the pure SrF$_2$ doped emission peak intensity shows obvious advantages. Compared with the previous at 500 °C optimal concentration (SrCO$_3$: SrF$_2$ = 3:7), it is found that the pure SrF$_2$ doped emission peak intensity is about 5 times, showing strong green emission. Fig. 4(d) shows the excitation spectrum at 460 °C. It can be seen from the figure that the CsPbBr$_3$ QDs microcrystals show a 300-500 nm wide excitation band, and the excitation peak intensity of pure SrF$_2$ doping is much higher than that of other F-doped QDs.
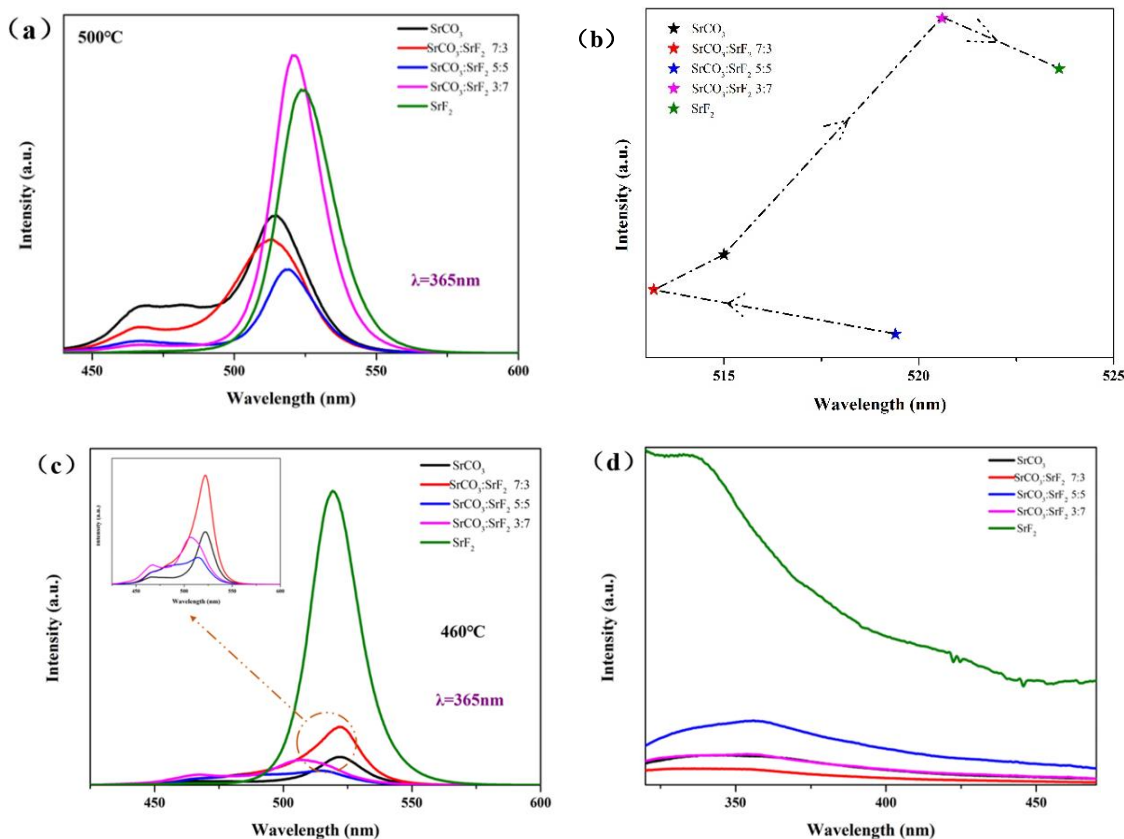
Fig. 4. (a) PL emission spectra of CsPbBr$_3$ doped with different F$^-$ at 500 °C heat treatment for 5h; (b)The emission peak position vertex chart; (c) PL emission spectra of CsPbBr$_3$ doped with different F$^-$ at 460 °C heat treatment for 5 h. Inset: other concentrations PL; (d) PLE at 460 °C heat treatment (color online)

In order to further understand the excellent fluorescence properties of pure SrF_2 doped $CsPbBr_3$ QDs microcrystals, the spectra at different heat treatment temperatures are shown in Fig. 5. From the emission spectrum can be seen that the QDs coated with pure SrF_2 doped borosilicate microcrystals show a narrow emission peak after heat treatment for 5 h, as shown in Fig. 5(a). When the heat treatment temperature is 460 °C, the emission peak is the highest, and the green emission at 519 nm is the strongest, as shown in Fig. 5(b). When the temperature rises from 440 °C to 500 °C, the position of the PL peak first moves from 498 nm to 525 nm, and the FWHM is 21–24 nm, indicating that the size distribution of the prepared sample is narrow. Besides, the peak shift reaches the limit at 480 °C, when the temperature rises to 500 °C, the peak shift does not occur, but the intensity of the peak decreases. When the temperature continues to rise to 520 °C, the emission peak moves from 525 nm to 520 nm with blue shifts [37]. The reason why the red shift occurs first is that when the temperature is low, the growth of QDs microcrystals in borosilicate is slow, the crystallinity is low and the reaction is not sufficient, generating the poor PLQY. When the temperature increases gradually, the reaction rate of QDs in the borosilicate matrix accelerates, which effectively promotes the formation of crystal and increases the PLQY. When the temperature is too high, the defects of the QDs will be quenched, which reduces the luminous efficiency, leading to the lower PLQY and the spectrum blue shift. Therefore, $CsPbBr_3$ QDs microcrystals the highest degree of crystallinity when heat-treated at 460 °C, which shows strong green light.
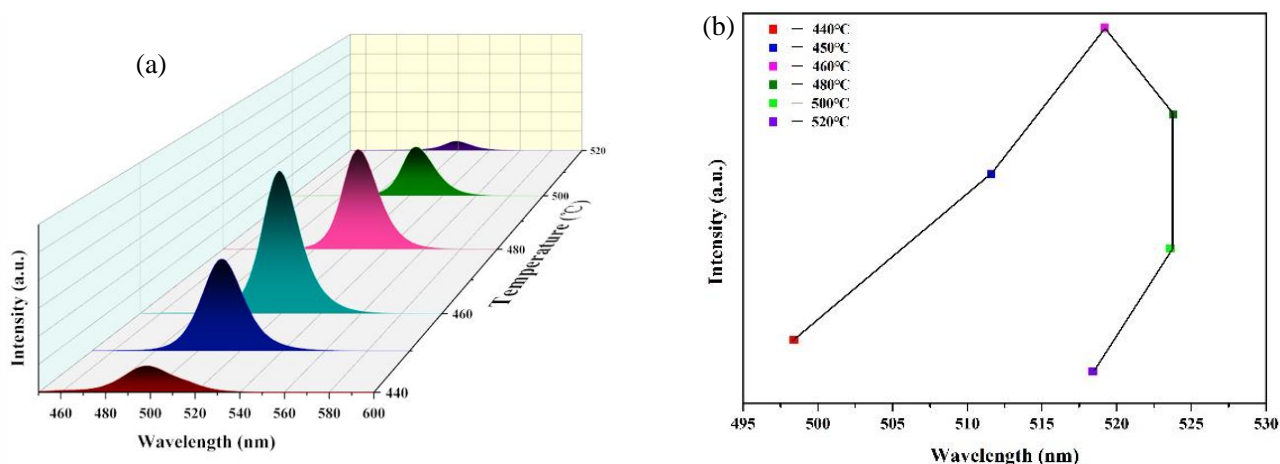
Fig. 5. (a) CsPbBr₃ QDs microcrystals emission spectra under different heat treatment for 5 h; (b) Emission peak location map for heat treatment at different temperatures (color online)

3.4. CIE chromaticity coordinate analysis

Fig. 6(a) is a picture of $CsPbBr_3$ QDs microcrystals excited by ultraviolet light at 365 nm after secondary heating. It can be seen that the luminescent intensity of QDs are blue-green after no treatment and low temperature (440 °C) treatment. With the increasing of temperature (440 °C ~500 °C), the luminescent intensity of QDs increases significantly. Especially when the temperature is 460 °C ~480 °C, the QDs microcrystals emit dazzling green light. It is confirmed that the emission peak intensity of the emission spectrum is high when the temperature is 460 °C ~480 °C, and the microcrystals begin to decrease when the temperature is further increased. Fig. 6(b) shows the chromatogram coordinates of $CsPbBr_3$ QDs microcrystals. When the temperature is too low, the color coordinates are displayed in the cyan blue region. At 440°C, the color coordinates are (0.0711,0.4394). At this time, the green light intensity of quantum-dot microcrystals is low. With the increase of temperature, the quantum-dots grow rapidly. At 450 °C, the color coordinates shift to the light green region, and the coordinates are (0.0721,0.9049). When the heat treatment temperature is 480 °C ～ 500 °C, the color coordinates move to (0.1472,0.7771) and (0.1486,0.7713). At this time, the color coordinates are in the dark green area, which has purer green light emission than the color coordinates of 440 °C～ 460 °C. When the temperature rises to 520 °C, the color coordinates move to (0.1049,0.6983), and the color coordinates are still in the green emission area. By studying the fluorescence decay lifetime of the samples, we can further understand the effects of different concentrations of F⁻ doping on their photo physical properties. Fig. 6(c) is the time-resolved lifetime curves of $CsPbBr_3$ QDs microcrystals doped with different F⁻ concentrations are fitted by a double exponential decay model. The model is calculated according to the following equation:

$$F(x) = A_1 * \exp(-\frac{x}{t_1}) + A_2 * \exp(-\frac{x}{t_2}) + C \qquad (1)$$

$$A_1 = t_1/(t_1 + t_2) \qquad (2)$$

$$A_2 = t_2/(t_1 + t_2) \qquad (3)$$

$$\tau = (A_1 t_1^2 + A_2 t_2^2)/(A_1 t_1 + A_2 t_2) \qquad (4)$$

The lifetime of pure SrF_2 doped microcrystals increases from a minimum of 4.04 ns to 14.42 ns, which enhances the lifetime decay time. Fig. 6(d) shows the

PLQY of different concentrations of F⁻ doping (record the samples as S1 ~ S5). When the concentration is pure SrF_2 doping, the quantum-yield is 44.81%, reaching the highest. It emits strong green light under 365 nm UV irradiation.

Therefore, the microcrystals of $CsPbBr_3$ QDs doped with fluorine can still emit green light with high intensity even at high temperature, which shows that such materials can still maintain their own excellent luminescent properties at high temperature, lying a foundation for the preparation of high-power, long-life powder solid-state luminescent devices in the future.
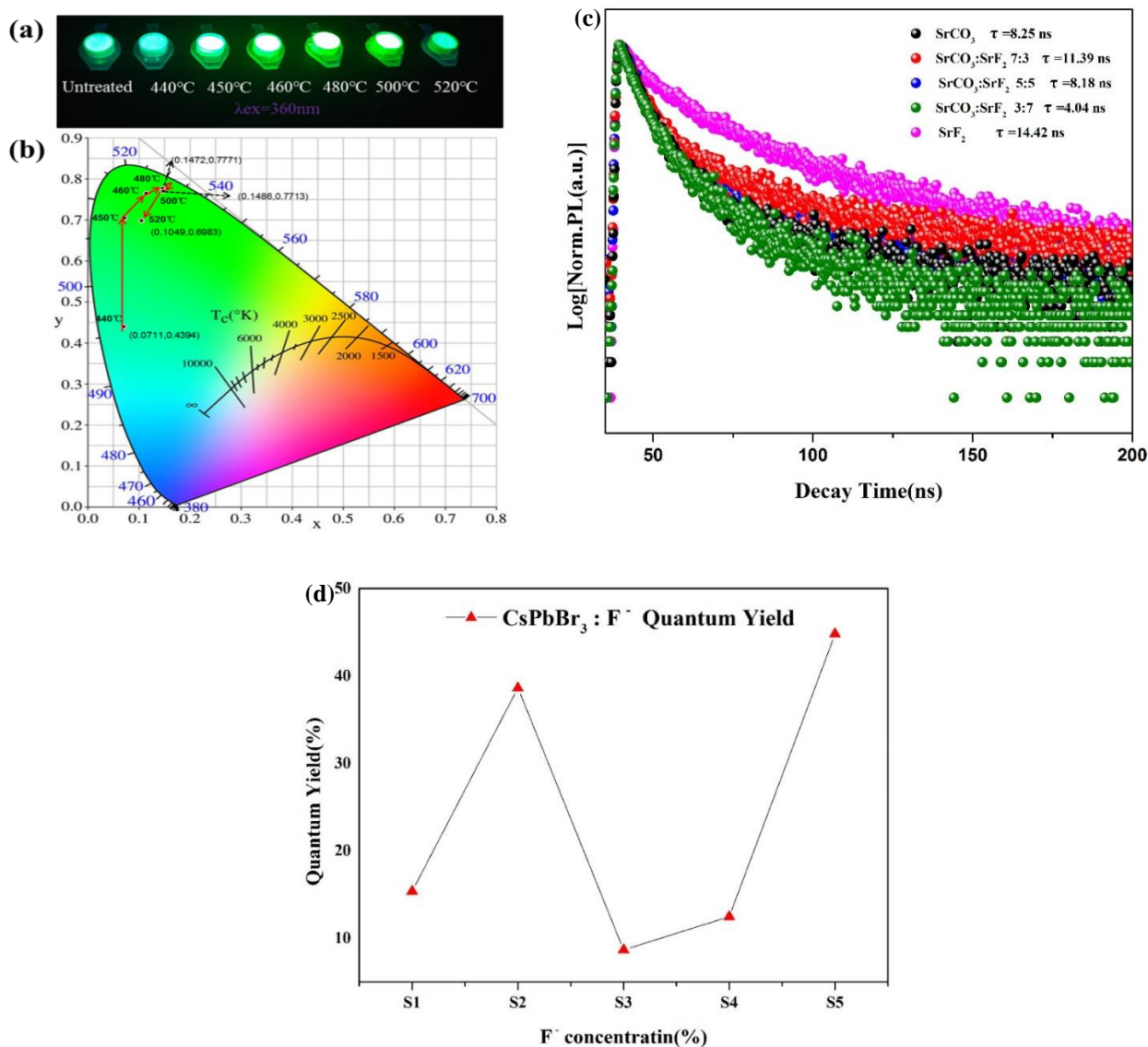
Fig. 6. (a) CsPbBr₃ QDs microcrystals physical picture at different temperatures; (b) CIE chromaticity coordinate diagram; (c) Time-resolved PL decay profiles of F-doped CsPbBr₃ QDs microcrystals; (d) The PLQY of CsPbBr₃: F⁻ QDs microcrystals (color online)

4. Conclusions

The effect of different concentrations fluorine doped borosilicate microcrystals on the optical properties of CsPbBr$_3$ QDs was investigated by a novel melting and cooling technology. XRD results confirmed that the QDs crystallites were successfully doped inside the borosilicate crystallites. TEM shows that the QDs are effectively formed in borosilicate microcrystals, and the average size of CsPbBr$_3$ QDs after statistics is 3.11 nm. The spectrum can be adjusted by controlling different reaction temperature, and the emission peak of QDs is extremely high at 460 °C. It can be seen from the CIE chromaticity coordinate diagram that when the temperature is between 480 °C and 500 °C, the fluorine doped borosilicate microcrystals exhibits strong green emission. When the temperature rises even higher, the color coordinates remain in the green emission region, which demonstrates the thermal stability of CsPbBr$_3$ QDs. The lifetime of pure SrF$_2$ doped microcrystals increases from a minimum of 4.04 ns to 14.42 ns, which enhances the lifetime decay time, and the PLQY increased to 44.81%. CsPbBr$_3$ QDs microcrystals show excellent luminescent properties and thermal stability, revealing great development prospect in the field of high-power, long-life powder solid-state lighting.

References

[1] Henry J. Snaith, J. Phys. Chem. Lett. **4**(21), 3623 (2013).

[2] S. S. Shin, E. J. Yeom, W. S. Yang, S. Hur, M. G. Kim, J. Im, J. Seo, J. H. Noh, S. I. Seok, Science **356**(6334), 167 (2017).

[3] S. H. Turren-Cruz, A. Hagfeldt, M. Salba, Science **362**(6413), 449 (2018).

[4] E. J. Juarez-Perez, Z. Hawash, S. R. Raga, L. K. Ono, Y. Qi, Energy Environ. Sci. **9**(11), 3406 (2016).

[5] M. Kulbak, S. Gupta, N. Kedem, I. Levine, T. Bendikov, G. Hodes, D. Cahen, J. Phys. Chem. Lett. **7**(1), 167 (2016).

[6] F. Palazon, Q. A. Akkerman, M. Prato, L. Manna, ACS Nano **10**(1), 1224 (2015).

[7] I. Lignos, S. Stavrakis, G. Nedelcu, L. Protesescu, A. J. DeMello, M. V. Kovalenko, Nano Letters **16**(3), 1869 (2016).

[8] Y. Cao, N. Wang, H. Tian, J. Guo, Y. Wei, H. Chen, Y. Miao, W. Zou, K. Pan, Y. He, H. Cao, Y. Ke, M. Xu, Y. Wang, M. Yang, K. Du, Z. Fu, D. Kong, D. Dai, Y. Jin, G. Li, H. Li, Q. Peng, J. Wang, W. Huang, Nature **562**(7726), 249 (2018).

[9] S. Kumar, J. Jagielski, N. Kallikounis, Y. H. Kim, C. Wolf, F. Jenny, T. Tian, C.J. Hofer, Y. C. Chiu, W.J. Stark, T. W. Lee, C. J. Shih, Nano Lett. **17**(9), 5277 (2017).

[10] L. Protesescu, S. Yakunin, M. I. Bodnarchuk, F. Krieg, R. Caputo, C. H. Hendon, R. Yang, A. Walsh, M. V. Kovalenko, Nano Lett. **15**(6), 3692 (2015).

[11] T. Chiba, Y. Hayashi, H. Ebe, K. Hoshi, J. Sato, S. Sato, Y.-J. Pu, S. Ohisa, J. Kido, Nat. Photon. **12**(11), 681 (2018).

[12] R. Begum, M. R. Parida, A. L. Abdelhady, B. Murali, N. M. Alyami, G. H. Ahmed, M. N. Hedhili, O. M. Bakr, O. F. Mohammed, J. Am. Chem. Soc. **139**(2), 731 (2016).

[13] Q.A. Akkerman, V. D'Innocenzo, S. Accornero, A. Scarpellini, A. Petrozza, M. Prato, L. Manna, J. Am. Chem. Soc. **137**(32), 10276 (2015).

[14] V. K. Ravi, G. B. Markad, A. Nag, ACS Energy Lett. **1**(4), 665 (2016).

[15] W. S. Yang, J. H. Noh, N. J. Jeon, Y. C. Kim, S. Ryu, J. Seo, S. I. Seok, Science **348**(6240), 1234 (2015).

[16] G. E. Eperon, S. D. Stranks, C. Menelaou, M. Johnston, L. Herz, H. Snaith, Energy Environ. Sci. **7**(3), 982 (2014).

[17] C. Y. Chen, H. Y. Lin, K. M. Chiang, W. L. Tsai, Y. C. Huang, C. S. Tsao, H. W. Lin, Adv. Mater. **29**(12), 1605290 (2017).

[18] R. E. Beal, D. J. Slotcavage, T. Leijtens, A. R. Bowring, R. A. Belisle, W. H. Nguyen, G. F. Burkhard, E. T. Hoke, M. D. McGehee, J. Phys. Chem. Lett. **7**(5), 746 (2016).

[19] P. Wang, X. Bai, C. Sun, X. Zhang, T. Zhang, Y Zhang, Appl. Phys. Lett. **109**(6), 063106 (2016).

[20] S. Jizhong, Li. Jianhai, Li. Xiaoming, Adv. Mater. **47**(4), 4 (2016).

[21] G. Li, Z. Tan, D. Di, M.L. Lai, L. Jiang, J. H. Lim, R. H. Friend, N. C. Greenham, Nano Lett. **15**(4), 2640 (2015).

[22] Y. H. Kim, H. Cho, J. H. Heo, T. S. Kim, N. Myoung, C. L. Le, S. H. Im, T. W. Lee, Adv. Mater. **27**(7), 1248 (2015).

[23] S. Yakunin, L. Protesescu, F. Krieg, Nat. Commun. M. Bodnarchuk, G. Nedelcu, M. Humer, L. De, M. Fiebig, W. Heiss, M. Kovalenko, Nat. Commun. **6**, 8056 (2015).

[24] Y. Wang, X. Li, J. Song, L. Xiao, H. Zeng, H. Sun, HD, Adv. Mater. **27**(44), 7101 (2015).

[25] R. Long, H. L. Wang, R. H. Cheng, Q. Gong, J. Y. Yan, Y. Wang, P. Chen, Z. T. Song, S. L. Feng, Chin. J. Lumin. **34**(4), 474 (2013).

[26] A. Sanduta, S. S. Rusu, V. Z. Tronciu, IFMBE Proceedings **55**, 179 (2016).

[27] P. Ramasamy, D. Lim, B. Kim, S. Lee, M. Lee, J. Lee, Chem. Commun. **52**, 2067 (2015).

[28] G. Walters, B. R. Sutherland, S. Hoogland, D. Shi, R. Comin, D. P. Sellan, O. M. Bake, E. H. Sargent, ACS Nano. **9**(9), 9340 (2015).

[29] H. Wang, S. Lin, R. S. Liu, B. Singh, H. Tong, C. Chen, Y. Lee, T. Tsai, R. Liu, Angew. Chem. **55**(28), 7924 (2016).

[30] B. Ai, C. Liu, J. Wang, J. Xie, J. Han, X. Zhao, J. Heo, J. Am. Ceram. Soc. **99**(9), 2875 (2016).

[31] P. T. Guerreiro, S. Ten, N. F. Borrelli, Appl. Phys. Lett. **71**(12), 1595 (1997).

[32] C. Liu, J. Heo, X. Zhang, J. L. Adam, J. Non Cryst. Solids. **354**(2-9), 618 (2008).

[33] A. Lipovskii, E. Kolobkova, V. Petrikov, I. Kang, A. Olkhovets, T. Krauss, M. Thomas, J. Silcox, F. Wise, Q. Shen, S. Kycia. Appl. Phys. Lett. **71**(23), 3406 (1997).

[34] D. Chen, Y. Liu, C. Yang, J. Zhong, S. Zhou, J. Chen, H. Huang, Nano. **11**(37), 17216 (2019).

[35] J. Wu, H. Bai, W. Qu, G. Cao, Y. Zhang, Opt. Mater. **97**, 109454 (2019).

[36] V. K. Ravi, A. Swarnkar, R. Chakraborty, A. Nag, Nanotechnology **27**(32), 325708 (2016).

[37] Y. Ye, W. Zhang, Z. Zhao, J. Wang, C. Liu, Z. Deng, X. Zhao, J. Han, Adv. Opt. Mater. **7**(9), 1801663 (2019).

---

*Corresponding author: gycao@dlpu.edu.cn;
zhang_yj@dlpu.edu.cn